

# Reactive experimental control of turbulent jets

Diego B. S. Audiffred<sup>1</sup>, André V. G. Cavalieri<sup>1</sup>, Igor A. Maia<sup>1</sup>, Eduardo Martini<sup>2</sup>  
and Peter Jordan<sup>2</sup>

<sup>1</sup>Instituto Tecnológico de Aeronáutica, São José dos Campos, São Paulo, Brazil

<sup>2</sup>Institut Pprime-CNRS-Université de Poitiers-ENSMA, Chasseneuil du Poitou, Nouvelle-Aquitaine, France

## Abstract

We present an experimental study of reactive control of turbulent jets. We target axisymmetric disturbances associated with coherent structures, which are known to underpin the peak sound radiation of turbulent jets. We first consider a forced jet flow case, such that the coherent structures can be amplified above background levels, which makes it easier to detect them by the sensors. We then consider the more challenging case of a natural jet, i.e., without artificial forcing. The control strategy explores linear convective mechanisms in the initial jet region, which justifies application of linear control theory. The control law is constructed in the frequency domain, based on empirically determined transfer functions. The Wiener-Hopf formalism is used to enforce causality, providing an optimal causal solution, thus, preventing the drop in performance that may be observed in flow control applications that use simpler wave-cancellation methods. With this approach, we could improve the control performance of forced turbulent jets compared to results obtained in previous studies, attaining order-of-magnitude attenuation of power spectra of velocity fluctuations. Furthermore, we could obtain substantial levels of attenuation of natural turbulent jets, of about 60% in power spectra for the most amplified frequencies. These results open new directions for the control of turbulent flows.

## 1. Introduction

Attenuation of jet exhaust noise is one of the main concerns of the aircraft industry. Since the introduction of jet engines, many studies have been conducted aiming at reducing jet exhaust noise (Wirt 1966; Seiner & Krejsa 1989; Saiyed *et al.* 2000; Ginevsky *et al.* 2004; Morris & McLaughlin 2019; Zigunov *et al.* 2022). However, jet noise still remains one of the main noise sources in an aircraft, and is dominant during takeoff (Leylekian *et al.* 2014; Huff *et al.* 2016). Furthermore, the Advisory Council for Aeronautics Research in Europe (ACARE) has established a goal of reducing the perceived noise emission of flying aircraft by 65% in 2050 with respect to the values observed in the year 2000 (European Commission 2011).

Jet noise generation is mainly caused by the high-velocity exhaust gases that leave the nozzle and meet the atmospheric air, which creates turbulence with a wide range of turbulent structures (Suzuki & Colonius 2006). Among these, there are large coherent flow structures (Mollo-Christensen 1967; Crow & Champagne 1971; Lau *et al.* 1972; Moore 1977), which are acoustically efficient and dominate the downstream sound radiation (Tam *et al.* 1996, 2008; Michalke 1983). These coherent structures, also known as wavepackets, are underpinned by the Kelvin-Helmholtz instability, and are characterized by a large spatial envelope of growth and decay, and a high degree of organization (Gudmundsson & Colonius 2011; Jordan & Colonius 2013; Cavalieri *et al.* 2019).

When it comes to reducing jet noise, lowering the jet velocity may be seen as the obvious

thing to do, since the total acoustic power is roughly proportional to  $U^8$ , as predicted by Lighthill (1952). In the last decades, larger engines were developed to increase efficiency. A consequence of a larger turbine is that, for a given thrust, the jet velocity can be reduced, also reducing the radiated noise. However this strategy is reaching its limits due to structural and ground clearance reasons. Therefore, to further reduce jet noise, it is important to explore new solution strategies (Leylekian *et al.* 2014). Another well-known noise-mitigation strategy consists in using modified nozzle geometries, such as chevron nozzles, which has been shown as an effective technology to reduce jet noise (Tide & Srinivasan 2009; Huff 2007). The mechanism behind the low-frequency noise reduction observed with chevron nozzles is the increase in streamwise vorticity in the jet shear layer. This enhances the mixing, reduces the potential core length as has a stabilizing effect on Kelvin-Helmholtz wavepackets (Alkisar *et al.* 2007; Sinha *et al.* 2016; Lajús *et al.* 2019). One advantage of such passive control devices is that they do not require an energy input. However, it typically leads to lower thrust efficiency. Another strategy is to use reactive flow control, where real-time sensor readings are used in order to build a control law and generate an unsteady actuation, which responds in real-time to unsteady fluctuations in the flow.

Since the main component responsible for jet noise generation are wavepackets, whose underlying dynamics can be modeled using linear models, especially near the nozzle exit (Cavaliere *et al.* 2013), the application of linear control theory is a suitable candidate for designing an explicit control law for jet noise attenuation. The first explicit attempt of actively controlling instability waves in jets was investigated in a 2D model of a nozzle edge, where the suppression of a time-harmonic instability wave was shown to be theoretically possible via an external acoustic excitation with properly chosen amplitude and phase (Kopiev & Faranosov 2008). Few years later, this was performed experimentally, where harmonically forced disturbances in a turbulent jet have been attenuated by an external acoustic source (Kopiev *et al.* 2013) and also with plasma actuators (Kopiev *et al.* 2014). This study evolved to the development of a strategy for controlling natural instability waves in subsonic turbulent jets (Belyaev *et al.* 2018), which was later tested experimentally in a feedback control scheme (Faranosov *et al.* 2019), where axisymmetric instability waves of a natural jet were attenuated using a plasma actuator placed inside the nozzle, near the exit. For such case, the control was only aimed at a Strouhal number of  $St = 0.46$ , and attenuation was achieved for a narrow frequency range around this target frequency. More recently, the Inverse Feed-forward Control (IFFC) method (Sasaki *et al.* 2018) was used in experimental control studies of band-limited stochastically forced turbulent jets, with the objective of canceling axisymmetric hydrodynamic wavepackets using synthetic jets actuators (Maia *et al.* 2021, 2022). Several studies were also developed focusing on the control of mixing layers, which can be seen as a simple model for the initial region of the jet shear layer (Wei & Freund 2005; Parezanović *et al.* 2014; Shaqarin *et al.* 2018).

The IFFC method opened the possibility of controlling disturbances in a broader spectrum, which was an important step towards the control of a turbulent jet. The IFFC approach is constructed in the frequency domain. When converted back to the time domain, this approach casts the control law as a convolution between sensor readings and a control kernel. In general, this convolution is non causal, i.e., it requires future information to construct the present flow actuation. Real-time applications require that only the causal part of the kernel (present and past measurements) be used. In IFFC, this is enforced by truncating the kernel to its causal part, which might result in a substantial drop in performance (Brito *et al.* 2021). This issue can be circumvented with the Wiener-Hopf formalism, which provides a framework to compute an optimal causal control kernel (Martinelli 2009; Martini *et al.* 2022). Recent numerical and experimental studies have shown that Wiener-Hopf-based control can improve on the results of IFFC for amplifier flows (Martini *et al.* 2022; Audiffred *et al.* 2023b). This suggests that the turbulent jet control can benefit from the Wiener-Hopf technique as well.

In the present work we aim at attenuating axisymmetric hydrodynamic wavepackets with the

application of the Wiener-Hopf technique in a turbulent jet. We first consider the case of a forced jet. The application of an external forcing increases the amplitudes of the targeted flow structures, making it easier to identify and control them (Crow & Champagne 1971; Moore 1977; Gudmundsson & Colonius 2011). This is the same underlying idea of the work by Maia *et al.* (2021). This avoids some of the difficulties of the control of a natural jet, and is a necessary first step to test the control strategy and provide a proof of concept of its suitability. Furthermore, we emphasise, that, as in Maia *et al.* (2021, 2022), forcing amplitudes are kept small enough so that the jet responds *linearly*. This makes sure that the instability mechanisms in the forced jet are essentially the same as in their natural counterparts. In the second part of the study, we extend the control approach to the natural jet case. As highlighted above, this is a more challenging scenario, due to the difficulty in sensing the low-energy axisymmetric wavepackets. A natural jet case is a condition of greater interest since turbulent jets in practice do not involve an explicit forcing.

The characteristics of the control experiment is discussed in the next section. In §3, the Wiener-Hopf technique is briefly presented, along with the control design considering both the Wiener-Hopf and the inverse feed-forward control methods. Then, the results obtained by each of these methods are compared and discussed in §4. Further discussion about the control applied and the results obtained are offered in §5, which concludes the paper.

## 2. Experimental Setup

Real-time flow control experiments of turbulent jets have been performed at the Pprime Institute. We consider jets at Mach number of 0.05 and a Reynolds number of  $Re = 5 \times 10^4$ . Transition to a fully turbulent jet was guaranteed by a strip of carborundum particles placed  $2.5D$  upstream of the nozzle exit plane, where  $D$  is the nozzle diameter, which is 50 mm. The experimental setup was based on the experiments reported by Maia *et al.* (2021), which is represented in fig. 1. It consisted of six microphones, working as pressure sensors, providing the axisymmetric pressure mode information, which is the input signal,  $y$ , for the control law. The axisymmetric pressure mode obtained for the unforced jet is shown in fig. 2. Spectra of the six microphones are very close to each other, indicating azimuthal homogeneity. The axisymmetric mode has only a small fraction of the power, but it is known to be related to the peak acoustic radiation of subsonic jets (Juve *et al.* 1979; Cavalieri *et al.* 2013).

The actuation,  $u$ , was provided by synthetic jets generated by a set of six speakers. These actuators primarily work through a blowing and suction process of zero-net mass flux that generate a train of vortices that moves away from the device's orifice due to self induced velocity (Wang & Feng 2018). Further downstream, on the jet center line, a hot wire has been used to take streamwise velocity measurements. The microphones were placed at a distance  $x/D = 0.3$  from the nozzle exit, the actuators at a distance  $x/D = 1.5$ , and the hot wire at  $x/D = 2$ . The radial distance of the microphones from the jet center line was  $r/D = 0.55$ , while the actuators were placed at a radial distance  $r/D = 0.7$ . These choices of positioning avoided intrusion of sensors and actuators in the jet plume, remaining nonetheless in the near field. The first set of control experiments was performed considering the application of an axisymmetric forcing,  $d$ , provided by synthetic jets generated by a set of eight speakers. The application of a forcing signal helps improving the coherence between sensors and actuators, and also allows us to compare some of the results obtained here with those obtained by Maia *et al.* (2021).

For the forcing, we have considered two configuration of band-limited stochastic signals, one in a Strouhal number range  $0.3 \leq St \leq 0.45$ , and the other for Strouhal numbers in the interval  $0.3 \leq St \leq 0.85$ . The actuation was designed in the same Strouhal number range as the forcing, as will be described in the next section. In the case of the unforced (natural) jet, the actuation is within the band  $0.3 \leq St \leq 0.85$ . This range corresponds, to a great extent, to the most amplified frequencies at the sensor position, due to the Kelvin-Helmholtz mechanism (Maia *et al.*

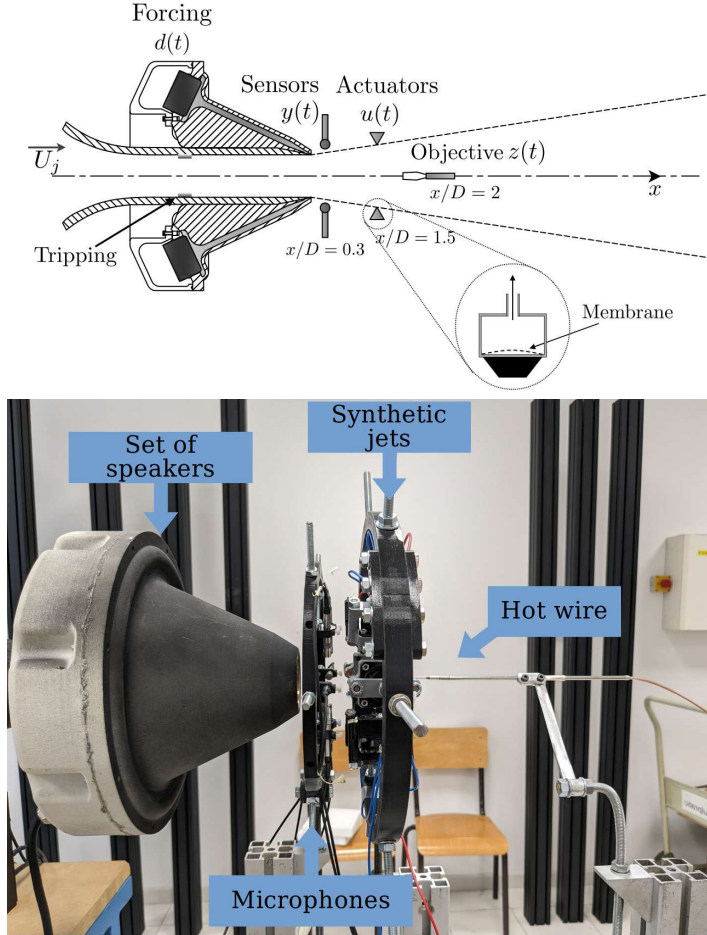


FIGURE 1. Sketch of the control scheme of the experimental setup, showing sensors and actuators positioning (Maia *et al.* 2021)(top), and a side view photo of the control setup (bottom).

2021, 2022). Further downstream, at the control target, growth rates are smaller, but the jet still remains convectively unstable up to  $St = 0.65$  (Maia *et al.* 2021). Therefore, the frequency range considered for the forcing falls within the unstable region of the spectrum. This is one of the ranges considered by Maia *et al.* (2021).

The Simulink tool, which is integrated with MATLAB, has been used to build the control model that was employed in the ControlDesk software from dSPACE, and the MicroLabBox system acquisition from dSPACE has been used for the real-time sensor readings and actuation, following the same procedure as earlier flow control works of our group (Brito *et al.* 2021; Audiffred *et al.* 2023b).

### 3. Control law design

#### 3.1. Overview of the Wiener-Hopf technique

The Wiener-Hopf technique (Noble 1958; Martini *et al.* 2022) is applied for the jet control problem, and its performance is compared to that of a wave-cancelling approach (Sasaki *et al.* 2018; Brito *et al.* 2021; Maia *et al.* 2021). The same control parameters and transfer functions are used for both methods. In this section, the Wiener-Hopf technique is briefly presented, and further

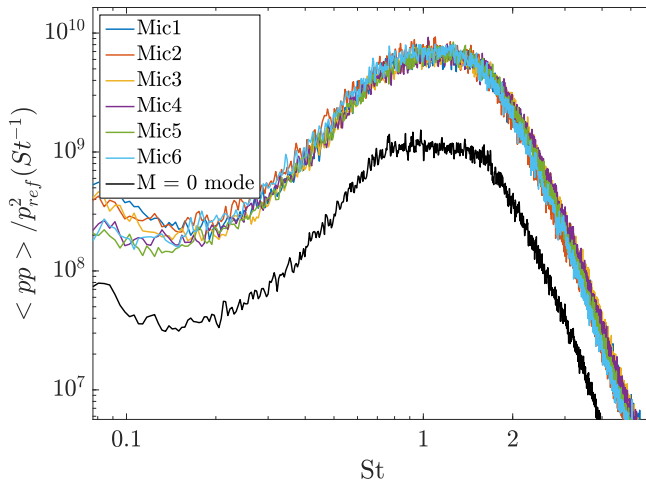


FIGURE 2. Pressure spectra measured by the six microphones and the resulting  $m = 0$  mode. Measurements taken at  $x/D = 0.3$  and  $r/D = 0.55$ .

details about this method and its application to control problems can be found in Martini *et al.* (2022). Wiener-Hopf equations are typically associated with problems where a half domain condition needs to be satisfied, such as a half-convolution problem (Noble 1958; Martini *et al.* 2022),

$$\int_0^{\infty} \hat{\mathbf{S}}(t - \tau) \mathbf{W}_+(\tau) d\tau = \mathbf{T}(t), \quad t > 0. \quad (3.1)$$

where  $\hat{\mathbf{S}}$  and  $\mathbf{T}$  are known functions and  $\mathbf{W}$  is a unknown function (kernel). Extending this equation for  $t < 0$ , and taking a Fourier transform, leads to the following equation in frequency domain:

$$\hat{\mathbf{S}}(\omega) \hat{\mathbf{W}}_+(\omega) = \hat{\mathbf{W}}_-(\omega) + \hat{\mathbf{T}}(\omega), \quad (3.2)$$

where  $+$  and  $-$  subscripts indicate that the function is analytical in the upper and lower complex half planes, respectively. This is ensured for  $\mathbf{W}_+$  and  $\mathbf{W}_-$  as these functions are defined to be zero for negative and positive times, respectively.  $\mathbf{W}_+$  and  $\mathbf{W}_-$  may also be referred to as causal and anticausal functions, respectively; these definitions carry over to all  $+$  and  $-$  functions.

Solution of such problem can be achieved with multiplicative and additive factorization,

$$\hat{\mathbf{S}}(\omega) = \hat{\mathbf{S}}_-(\omega) \hat{\mathbf{S}}_+(\omega), \quad (3.3)$$

$$(\hat{\mathbf{S}}_-^{-1}(\omega) \hat{\mathbf{T}}(\omega)) = (\hat{\mathbf{S}}_-^{-1}(\omega) \hat{\mathbf{T}}(\omega))_+ + (\hat{\mathbf{S}}_-^{-1}(\omega) \hat{\mathbf{T}}(\omega))_-. \quad (3.4)$$

Here, the multiplicative factorization of  $\hat{\mathbf{S}}(\omega)$  is solved numerically, based on the work done by Daniele & Lombardi (2007). With these two factorizations mentioned above, the solution of Eq. (3.1) is given by equations (3.5) and (3.6):

$$\hat{\mathbf{W}}_+(\omega) = \hat{\mathbf{S}}_+^{-1}(\omega) (\hat{\mathbf{S}}_-^{-1}(\omega) \hat{\mathbf{T}}(\omega))_+, \quad (3.5)$$

$$\hat{\mathbf{W}}_-(\omega) = \hat{\mathbf{S}}_-(\omega)(\hat{\mathbf{S}}_-^{-1}(\omega)\hat{\mathbf{T}}(\omega))_-, \quad (3.6)$$

$\hat{\mathbf{W}}_+$ , which is regular in the upper-half complex plane, it is the term related to causal control.

### 3.2. Control law design based on the Wiener-Hopf approach

The Wiener-Hopf based control is considered for a linear dynamical system. An optimal control for such system can be obtained by means of a quadratic cost functional that expresses the control cost and the cost of state deviation from original condition, where this functional is minimized with respect to the control kernel. For simplicity, we first consider a case without feedback contamination i.e., the effect of  $u$  on  $y$  is neglected. Causality can be enforced by including Lagrange multipliers to the quadratic cost functional,

$$J = \int_{-\infty}^{\infty} (\langle Qz^*z + Ru_+^*u_+ \rangle) dt + \int_{-\infty}^{\infty} [\Gamma_+(t)\Lambda_-(t)]dt + \int_{-\infty}^{\infty} [\Gamma_+^*(t)\Lambda_-^*(t)]dt, \quad (3.7)$$

where the \* superscript denotes the complex conjugate,  $z$  is the target for the control problem,  $Q$  is a weighting of the state deviation from original condition,  $R$  is a control penalisation,  $\Lambda_-$  is a Lagrange multiplier,  $\Gamma$  is the control kernel, and  $u$  is the actuation signal defined in frequency domain by eq. (3.8). As  $\Lambda$  is anticausal, the two last integrals in eq. (3.7) force  $\Gamma$  to be causal.

$$\hat{\mathbf{u}}(\omega) = \hat{\mathbf{\Gamma}}(\omega)\hat{\mathbf{y}}(\omega) \quad (3.8)$$

In the time domain, the actuation is given by the following convolution,

$$\mathbf{u}(t) = \int_{-\infty}^{\infty} \Gamma(\tau)\mathbf{y}(t - \tau)d\tau, \quad (3.9)$$

which can lead to a non-causal kernel if the causality restriction is not imposed by the Lagrange multipliers. When Eq. (3.7) is solved for the optimal solutions in the frequency domain, the following Wiener-Hopf equation is obtained:

$$\hat{H}_l\hat{\Gamma}_+\hat{S}_{yy} + \hat{\Lambda}_- = \hat{H}_r\hat{S}_{yz}, \quad (3.10)$$

where:

$$\hat{H}_l(\omega) = \hat{G}_{uz}^*(\omega)Q\hat{G}_{uz}(\omega) + R, \quad (3.11)$$

$$\hat{H}_r(\omega) = -\hat{G}_{uz}^*(\omega)Q, \quad (3.12)$$

$\hat{S}_{yy}(\omega)$  is the power spectral density (PSD) of the input signal  $y$  and  $\hat{S}_{yz}(\omega)$  is the cross-spectral density (CSD) between the observation signal  $y$  and the target signal  $z$  without actuation;  $G_{uz}$  is the transfer function from the control signal  $u$  to the output  $z$ . Applying the factorization presented earlier, the following expression is obtained for  $\hat{\Gamma}_+$ ,

$$\hat{\Gamma}_+ = \hat{S}_{yy+}^{-1}(\hat{S}_{yy-}^{-1}\hat{S}_{yz}\hat{H}_r\hat{H}_l^{-1})_+\hat{H}_l^{-1}. \quad (3.13)$$

The expression above is thus used for obtaining the optimal causal control law under the Wiener-Hopf formalism (Noble 1958; Martinelli 2009; Martini *et al.* 2022).

In the present system there is a feedback contamination of the sensors,  $y$ , by the actuators,  $u$ , due to their proximity in the experimental setup. To account for this effects, and avoid appearance of a Larson effect (Sanfilippo & Valle 2013), the Wiener-Hopf kernel is modified as shown below (Martini *et al.* 2022):

$$\hat{\Gamma}'_+ = (I + \hat{\Gamma}\hat{G}_{uy})^{-1}, \quad (3.14)$$

where  $\hat{G}_{uy}$  is the transfer function between the actuation signal and the microphone readings.

### 3.3. Control law design based on the inverse feed-forward control method

In the wave-cancelling approach, here also referred to as inverse feed-forward control method, the strategy for control involves a direct superposition of the predicted uncontrolled disturbance at the objective position with the actuation. The IFFC control law can be obtained by minimizing a quadratic functional cost, similar to what is shown in Eq. (3.7), but without the constraints imposed to obtain a causal kernel, i.e., without the Lagrange multiplier terms, which yields the following equation (Sasaki *et al.* 2018; Brito *et al.* 2021):

$$\hat{\Gamma} = \frac{(\hat{G}_{uz})^* Q \hat{G}_{yz}}{(\hat{G}_{uz})^* Q (\hat{G}_{uz}) + R}, \quad (3.15)$$

where  $\hat{G}_{yz}$  is the transfer function between the microphones  $y$  and the control target  $z$ , which is simply  $\hat{S}_{yz}/\hat{S}_{yy}$ . Once the inverse Fourier transform of the IFFC kernel is taken, the non-causal part is neglected, i.e, we consider  $\Gamma(\tau < 0) = 0$  in order to be able to apply the IFFC kernel in experiments.

In order to account for the contamination of the sensor readings caused by the actuators, it is also necessary to take into consideration the transfer function between the actuators and the microphones ( $G_{uy}$ ), in this case the IFFC kernel can be obtained as

$$\hat{\Gamma} = \frac{(\hat{G}_{uz} - \hat{G}_{uy}\hat{G}_{yz})^* Q \hat{G}_{yz}}{(\hat{G}_{uz} - \hat{G}_{uy}\hat{G}_{yz})^* Q (\hat{G}_{uz} - \hat{G}_{uy}\hat{G}_{yz}) + R}. \quad (3.16)$$

### 3.4. Further considerations about the control laws

For the present work the CSDs and PSDs were obtained using the Welch method, where the Hanning window has been considered with 218 blocks and 50% overlap. Since we have considered a sampling rate of 10 kHz ( $St = 29.9$ ) and measurements of 30 s to identify the transfer functions, we obtained a frequency resolution of 11 Hz ( $St = 0.03$ ), with a total of 2730 data points per block.

To remove some of the undesired noises from the kernel, a zero-phase band-pass filter was applied to the raw data before the calculation of the transfer functions. The application of a filter was important because even very small amplitude noise in the kernel could result in a rapidly increase of the actuation amplitudes due to the acoustic feedback contamination. A frequency-based control penalisation was used for the control kernels, wherein large penalisations were applied outside the desired frequency-band, defined previously. This helps avoiding undesired frequencies that can lead to feedback contamination and it also regularizes the problem, avoiding divisions by zero (or by values close to zero) in eqs. (3.13) and (3.15). To further regularize the problem, a noise term of constant value ( $1 \cdot 10^{-4}$ ) was added to the PSDs of  $u$  and  $y$ . For the case where a forcing is applied up to Strouhal number of 0.85, better results were obtained using a constant value of ( $1 \cdot 10^{-3}$ ).

The expressions used to obtain the control penalisation are shown in Eqs. (3.17-3.19),

$$R_1 = R_{ctrl} + a(R_{noise} - R_{ctrl})(\tanh(f + f_{c1}) - \tanh(f - f_{c1})), \quad (3.17)$$

$$R_2 = R_{ctrl} + a(R_{ctrl} - R_{noise})(\tanh(f + f_{c2}) - \tanh(f - f_{c2})), \quad (3.18)$$

---

	Frequency range	$f_{c1}$	$f_{c2}$	$R_{ctrl}$	$R_{noise}$
Forced jet	$(0.3 \leq St \leq 0.45)$	0.20	0.55	$1 \cdot 10^{-5}$	1
Forced jet	$(0.3 \leq St \leq 0.85)$	0.25	0.95	$3 \cdot 10^{-2}$	2
Natural jet	$(0.3 \leq St \leq 0.85)$	0.20	0.95	$1 \cdot 10^{-5}$	1

---

TABLE 1. Parameters considered for the control penalisation.

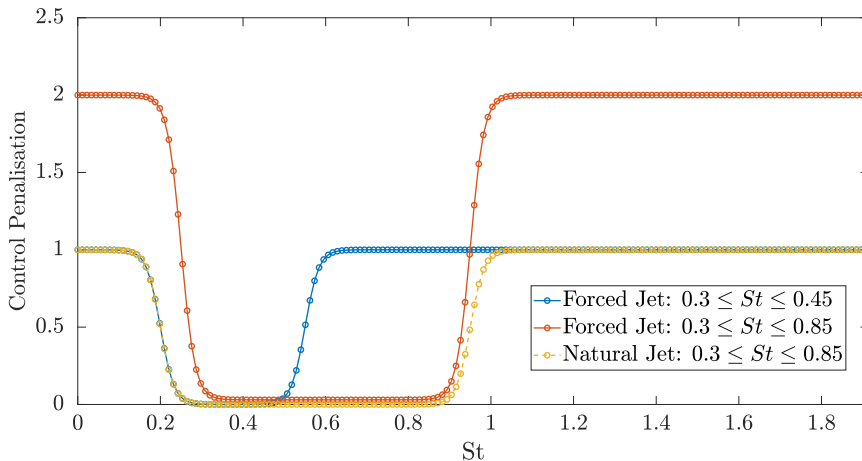


FIGURE 3. Control penalisation as function of the frequency.

$$R = \begin{cases} R_1, & \text{if } f_c \leq (f_{c1} + f_{c2})/2 \\ R_2, & \text{otherwise} \end{cases} \quad (3.19)$$

and are illustrated in fig. 3. Where  $f$  is a frequency vector;  $f_{c1}$  and  $f_{c2}$  are cut-off frequencies;  $R_{ctrl}$  defines the penalisation within the region of interest;  $R_{noise}$  is the penalisation out of the region of interest; We have used  $a = 30$ , which is a parameter that defines how fast and smooth is the transition from  $R_{ctrl}$  to  $R_{noise}$ . The parameters used in each case are summarized in table 1.

The functions related to the actuation ( $\hat{G}_{uy}$  and  $\hat{G}_{uz}$ ) were obtained with the forcing off, while  $S_{yy}$  and  $S_{yz}$  were obtained with the forcing (for the forced jet cases) on and the actuation off. The coherence obtained between the sensors and actuators are shown in fig. 4. High coherence levels are required for the linear control approaches employed used here.

As can be observed in the forced jet case, with the increase of the bandwidth significant lower coherence levels, between the reference sensors and the target, were observed for Strouhal numbers below 0.45. For  $St = 0.37$ , for example,  $\gamma_{yz}$  dropped by about 50% with the larger forcing bandwidth. For the forced jet with  $0.3 \leq St \leq 0.45$ ,  $\gamma_{yz}$  can also be considered relatively low for  $St = 0.34$  and lower, where  $\gamma_{yz}$  was below 0.6. This lower coherences can be explained either by the microphones not being able to properly identify the  $m = 0$  structures, e.g., due to azimuthal aliasing, or due to decoherence of the wavepacket along the jet. Unlike transitional flows, characterised by small disturbances, we deal here with a turbulent jet, with coherent structures that nonetheless display an intrinsic coherence decay, imposing additional challenges for flow control. Nevertheless, for the forced jet cases, the coherence between sensors were mostly above 0.8 for the frequencies of interest. Regarding the natural jet case, low coherence levels were obtained for the entire frequency range considered for control, around 0.5, which

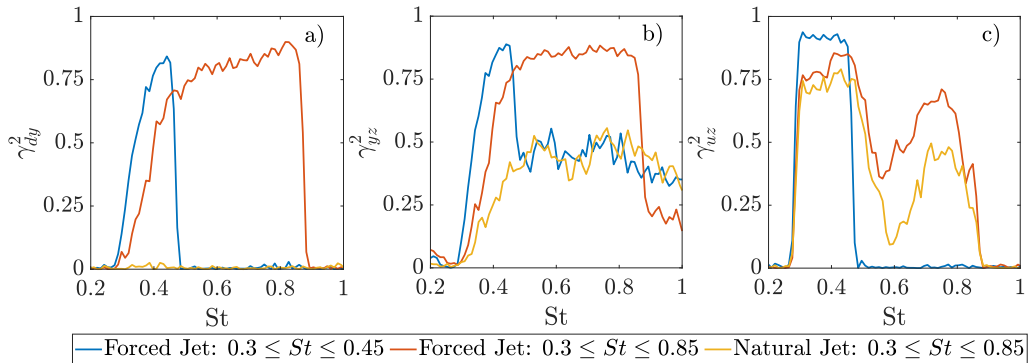


FIGURE 4. Coherence between: (a) forcing,  $d$ , and reference signal,  $y$ ; (b) reference signal,  $y$ , and control target,  $z$ , and; (c) actuation signal,  $u$ , and control target,  $z$ .

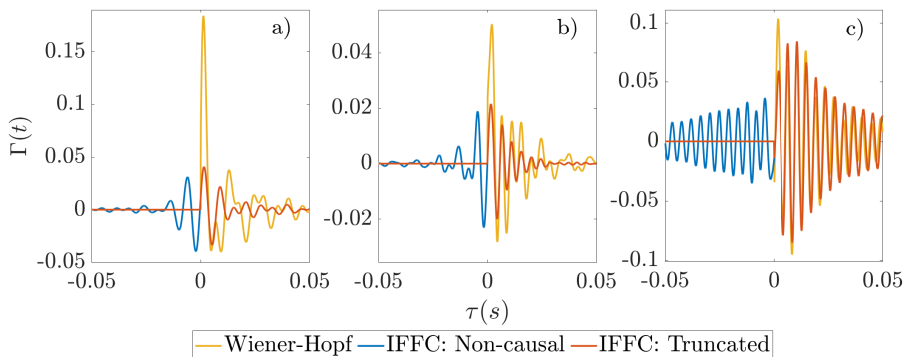


FIGURE 5. Control kernels in time domain for the forced jets (a)  $0.3 \leq St \leq 0.45$  (b)  $0.3 \leq St \leq 0.85$ , and (c) for the natural jet (actuation bandwidth =  $0.3 \leq St \leq 0.85$ ).

makes the control of natural turbulent jets a much more challenging task. The coherence between the actuation signal and the hot wire was higher than 0.85 for the region of interest, mostly above 0.9, when considering the forced jet case with  $0.3 \leq St \leq 0.45$ . However, as the actuation bandwidth increases, lower coherence levels are obtained, which was found to be a limitation of the actuation system. Differences in coherence levels observed between the forced and unforced cases ( $0.3 \leq St \leq 0.85$ ) can be partially explained by differences in the amplitudes of the actuation signals when identifying the transfer functions, but it was observed that this does not have a significant impact in the obtained kernel.

## 4. Results

### 4.1. Control laws

The kernels obtained with the inverse feed-forward control (IFFC) method and the Wiener-Hopf technique, which were discussed in the previous section, are compared in fig. 5 and 6.

In practical applications, it is unfeasible to apply the non-causal part of the IFFC kernel ( $\tau < 0$ ) shown in figure 5. For that reason, the non-causal kernel needs to be truncated to its causal part, i.e., we set  $\Gamma(\tau < 0) = 0$ , which reduces the performance of the controller. The Wiener-Hopf approach provides an optimal truncation strategy, minimizing the performance loss imposed by the causality constrain. The kernels obtained for the natural jet contain oscillations that do not decay to zero, as would be expected (Hervé *et al.* 2012; Fabbiane *et al.* 2015; Borggaard *et al.*

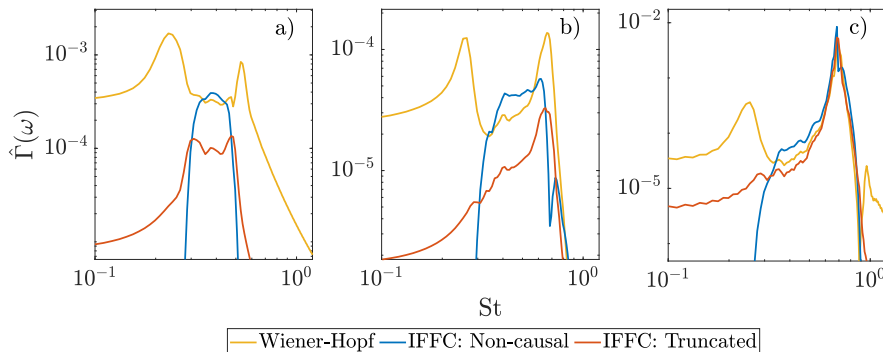


FIGURE 6. Control kernels in frequency domain for the forced jets (a)  $0.3 \leq St \leq 0.45$ , (b)  $0.3 \leq St \leq 0.85$ , and (c) for the natural jet (actuation bandwidth =  $0.3 \leq St \leq 0.85$ ).

2016; Karban *et al.* 2023), in this case they display a harmonic-like signature, due to the peak in  $\Gamma(\omega)$  around  $St=0.65$ . This is a way for the controller to compensate the low actuator-objective coherence (fig. 4c). This tonal behaviour results in the slow decay  $\Gamma(t)$ . For the forced jet cases, as the flow is driven by a stochastic signal, the coherent time-lengths are dominated by the forcing signal, not by the intrinsic flow dynamics.

Wiener-Hopf kernels present higher amplitudes at  $\tau \approx 0$ , which is seen as a compensation to the non-causality observed in the IFFC kernels, as observed in Martini *et al.* (2022) and Audiffred *et al.* (2023b). When observing the spectra of the kernels, figure 6, one may notice that the energy content of the Wiener-Hopf kernels, for the forced cases, is similar to the non-causal ones in the region we are aiming the control, while the truncated non-causal solution has considerably lower energy content in this same region, about 70% lower for both forced jet conditions. On the other hand, some undesired peaks out of the region of interest appeared for the Wiener-Hopf kernels. That likely occurs because we are exciting the jet flow with a band-limited stochastic forcing instead of a white noise. Additionally, the raw data is filtered in order to remove some of the noise present in the region we are not aiming the control, as mentioned earlier. The higher control penalisation for this same region prevents that those peaks extend for a larger bandwidth. Those peaks could be attenuated by modifying the cut-off frequencies in equations 3.17 and 3.18, but that would negatively affect the performance of the kernel.

#### 4.2. Control results

The control results obtained with the kernels presented above are shown in fig. 7, which displays the average PSDs of the objective, obtained from 3 measurements of 15 s each, with a sampling frequency of 10 kHz. In Audiffred *et al.* (2023a) we demonstrated, using this same data set, the control authority, i.e., that the reductions obtained are due to reactive control, not due to changes in the flow dynamics. The same has been already demonstrated by Maia *et al.* (2021).

For the forced jet cases, a significantly better performance is observed with the Wiener-Hopf kernel in comparison with the IFFC law. Here, the IFFC kernel had a worse performance than reported by Maia *et al.* (2021). In the present study we noticed that the actuator-objective transfer function,  $G_{uz}$ , was significantly different from that of Maia *et al.* (2021). This suggests a difference in actuator placement, or in the intrinsic mechanical characteristics of the actuation system. In any case, the Wiener-Hopf kernel still performed better than what is reported by Maia *et al.* (2021). For the case where a forcing is applied for  $0.3 \leq St \leq 0.45$ , a large peak is observed for the Wiener-Hopf results at Strouhal number around 0.52. Although this is undesired, the peak appears outside the frequency range we are aiming to control. This undesired peak resulted from one of the peaks observed in the Wiener-Hopf control kernel. For the case with larger forcing bandwidth,

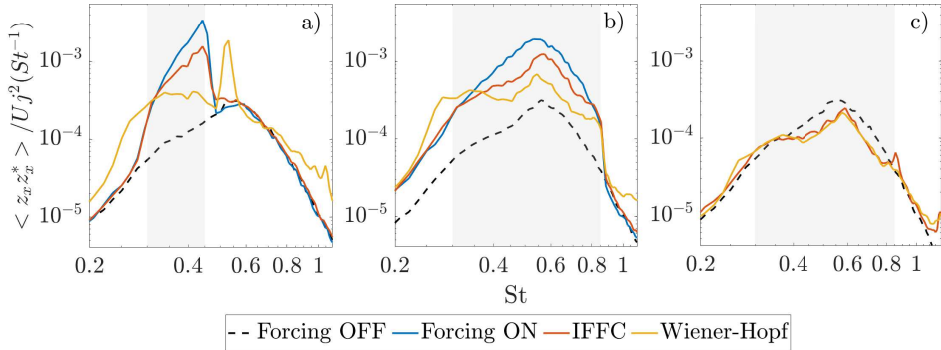


FIGURE 7. Spectra of the uncontrolled and controlled turbulent jet flow comparing the Wiener-Hopf and IFFC at the control target location, for the kernels obtained for the forced jets (a)  $0.3 \leq St \leq 0.45$ , (b)  $0.3 \leq St \leq 0.85$  and (c) unforced jet, with the control aimed for  $0.3 \leq St \leq 0.85$ .

we have observed a considerable increase in the broadband noise outside the frequency range of the excitation signal, which has also been observed in earlier studies (Moore 1977; Maia *et al.* 2021). For the natural jet, similar results were obtained with both control methods considered here, with an attenuation of power spectral density of about 40%, comparing the uncontrolled and controlled spectra, for the  $St$  range of higher amplification of the axisymmetric pressure mode.

#### 4.3. Downstream persistence of control effects

We also verified whether the control effect persisted downstream of the target position for the forced jet case with  $0.3 \leq St \leq 0.45$  and for the natural jet. A significant attenuation of the signals could still be observed until the streamwise position  $x/D = 7$ , as shown in figs. 8 and 9. For the forced case, we can observe that the Wiener-Hopf approach had a more positive impact for frequencies closer to the upper limit of the targeted frequency range compared to the IFFC approach, such that no forcing effect is visible for the Wiener-Hopf results at  $x/D = 7$ . For the natural jet, reductions of about 25% can be observed in the velocity spectra at  $x/D = 7$ , showing that control benefits are not restricted to the target location

#### 4.4. Improvement on sensor placement

As observed in fig. 4, the coherence between sensors drops significantly in the absence of a forcing applied to the jet. Since the amplitude of wavepackets increases as they are convected by the jet, it becomes easier to detect them. Thus, we considered positioning the array of microphones at a slightly downstream position, at  $x/D = 0.58$ , remaining nonetheless close to the nozzle. With this, we also changed the radial position of the sensors, moving them to  $r/D = 0.6$ , due to the thicker shear layer at that position. A comparison between the coherence between the target sensor  $z$  and the two positions of  $y$  sensors is shown in fig. 10, confirming that the downstream  $y$ -sensor placement leads to higher coherence and thus better estimation capabilities.

Since the coherence is still low for  $St < 0.45$ , we decided to restrict the actuation signal to the range  $0.45 \leq St \leq 0.9$ . The kernels for these new conditions are shown in fig. 11. With this higher coherence, the obtained kernels became less oscillatory than the ones presented in fig. 5, and the kernel signal has a stronger decay over time, as usual in flow control applications (Hervé *et al.* 2012; Fabbiane *et al.* 2015; Borggaard *et al.* 2016; Karban *et al.* 2023).

The spectra of the uncontrolled and controlled signals obtained with these new kernels are presented in fig. 12 for the objective position and in fig. 13 for measurements taken farther downstream. With the Wiener-Hopf kernel, at the objective position, reductions of more than 60% of power spectral density could be obtained for the most amplified frequencies. Attenuation

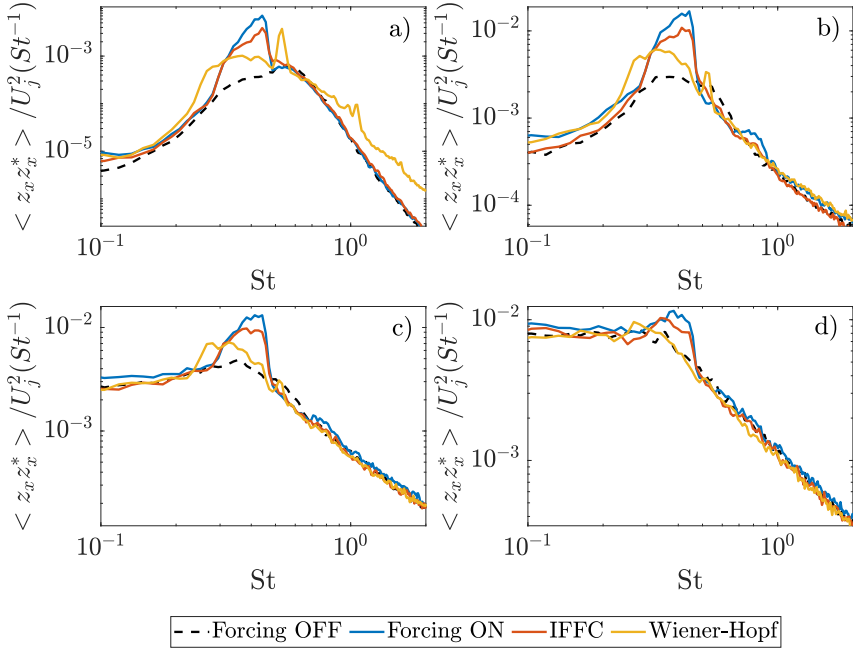


FIGURE 8. Spectra of the uncontrolled and controlled forced jet flow ( $0.3 \leq St \leq 0.45$ ) at different positions in the streamwise direction: (a)  $x/D = 2.5$ , (b)  $x/D = 5$ , (c)  $x/D = 6$ , (d)  $x/D = 7$ .

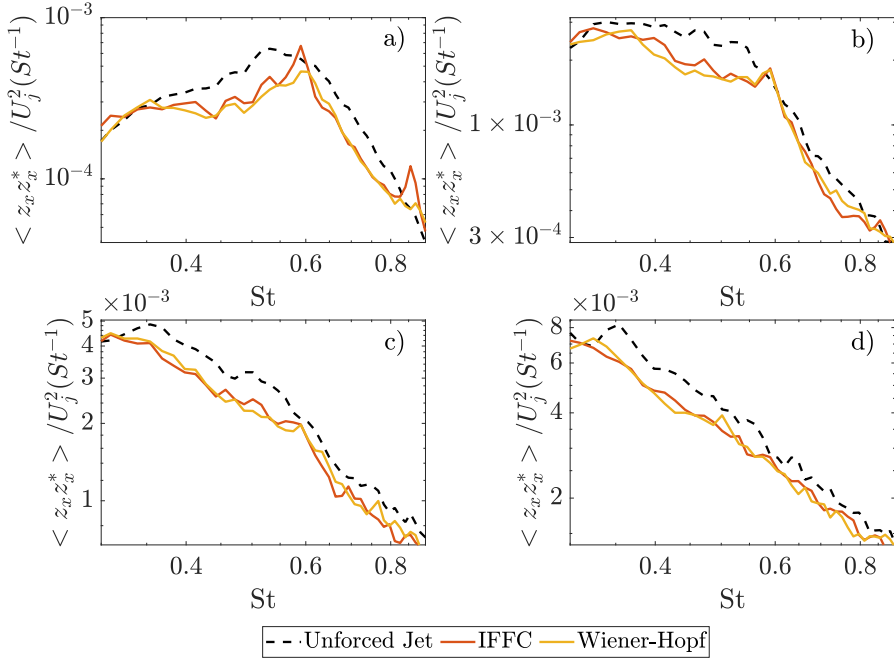


FIGURE 9. Spectra of the uncontrolled and controlled natural jet flow at different positions in the streamwise direction: (a)  $x/D = 2.5$ , (b)  $x/D = 5$ , (c)  $x/D = 6$ , (d)  $x/D = 7$ .

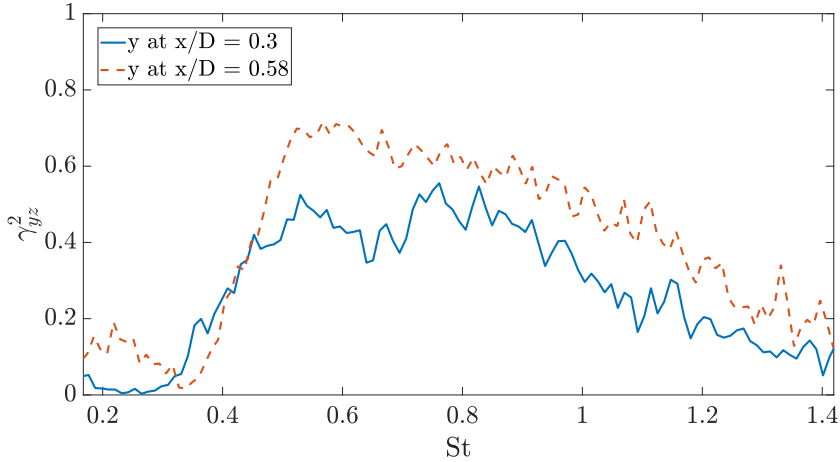


FIGURE 10. Coherence between the microphones and the hot wire, comparing the case with the microphones at  $x/D = 0.3$  and at  $x/D = 0.58$ .

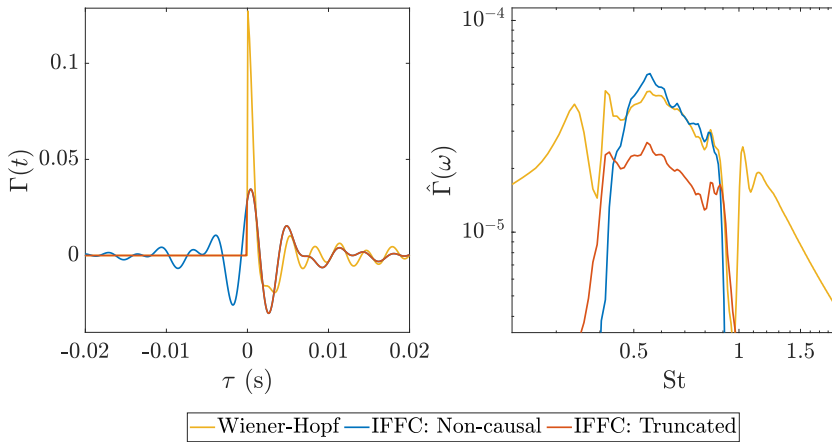


FIGURE 11. Control kernels of the unforced jet with the sensors farther downstream, in (a) time domain and (b) frequency domain.

close to that could also be obtained with the IFFC kernel, however, a much worse performance is observed at Strouhal number around 0.58. We also considered here a steady actuation case, where the actuators provide a band-limited stochastic signal with the same frequency range targeted by the reactive control, from where can be noticed that a simply steady actuation cannot guarantee the attenuation of the wavepackets, on the contrary, we had a condition where it amplifies the coherent structures.

When the reference sensors get closer to the actuators, the non-causal part of IFFC kernels increases, which deteriorates the performance of the truncated kernel, as reported in Martini *et al.* (2022) and by Audiffred *et al.* (2023b). The worse performance of the IFFC kernel at Strouhal number around  $St = 0.58$  seems also to be related to the low coherence presented by the actuator for this same region (fig. 4), where the Wiener-Hopf kernel was able to compensated that, most likely due to an overall stronger effort of the actuation.

We also evaluated the overall performance of the kernels, at different streamwise positions, in terms of the root mean square (RMS) of velocity fluctuations of the controlled and uncontrolled

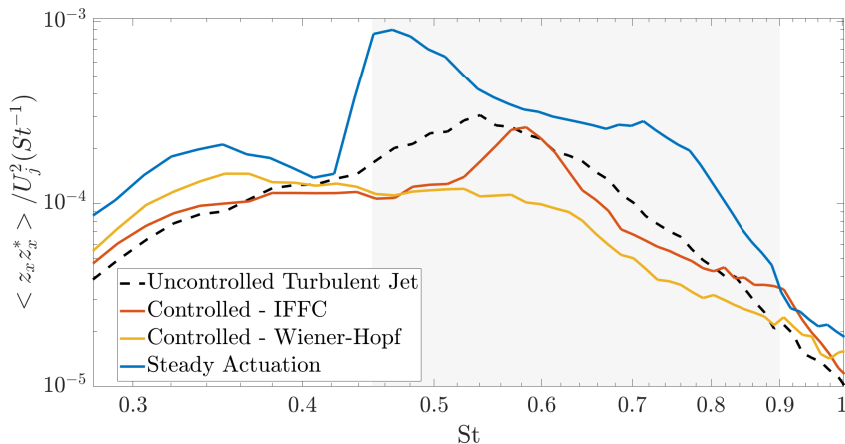


FIGURE 12. Spectra of the uncontrolled and controlled turbulent jet flow comparing the Wiener-Hopf and IFFC at the control target location.

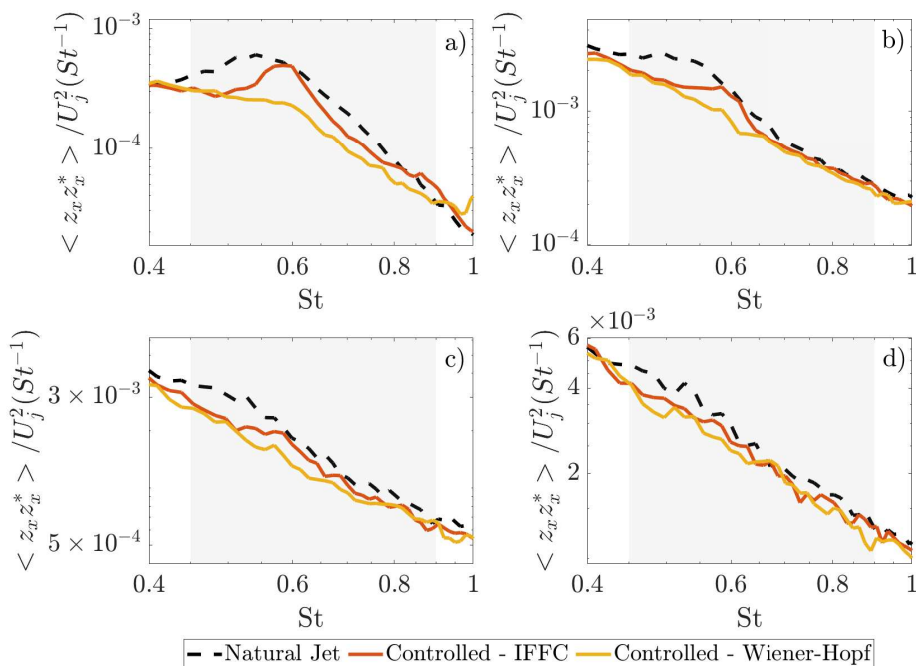


FIGURE 13. Spectra of the uncontrolled and controlled turbulent jet flow (for  $y$  at  $x/D = 0.58$ ), at different positions in the streamwise direction: (a)  $x/D = 2.5$ , (b)  $x/D = 5$ , (c)  $x/D = 6$ , (d)  $x/D = 7$ .

signals. The result of this, for the unforced case with the sensors farther downstream, is shown in fig. 14. The Wiener-Hopf kernel could provide a reduction of 28% of the RMS of the velocity fluctuations at the target location, which represents an overall reduction of 50% if we consider the integral of the PSDs over the target frequency range, instead of the RMS signal. On the other hand, the IFFC approach provided a RMS reduction of 12%. The performance of the IFFC kernel reaches a peak at  $x/D = 4$ , with a RMS reduction of 16%. Farther downstream, it is observed a linear decay of the control effect.

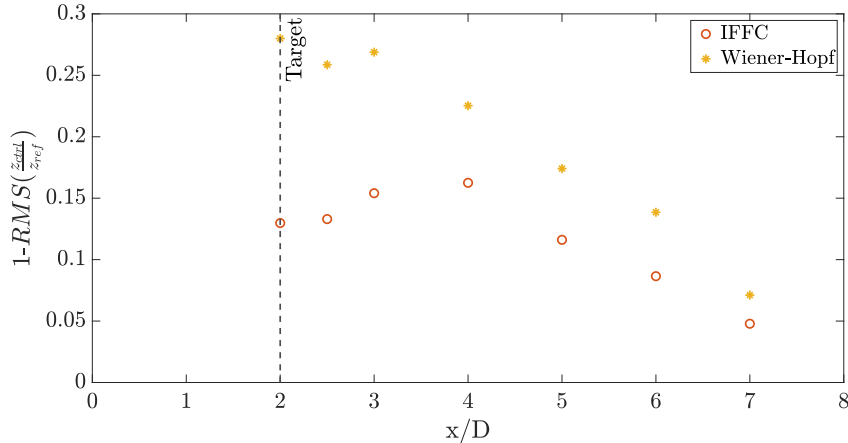


FIGURE 14. Relative performance of the control kernels, in terms of the  $RMS$  of velocity fluctuations of the controlled signals at different positions.

## 5. Conclusion

This work presented an experimental campaign on reactive control of turbulent jets, where a Wiener-Hopf approach was used to obtain the control kernels, while the inverse feed-forward control method was used as comparison. The control law aims at the attenuation of axisymmetric disturbances associated with Kelvin-Helmholtz wavepackets, known to be related to the peak subsonic jet noise (Jordan & Colonius 2013). The Wiener-Hopf-based control improves on previous results reported by Maia *et al.* (2021), for turbulent jets forced stochastically. Furthermore, we extend the control experiments to natural unforced jets; this is the first time, to the best of our knowledge, that reactive control is performed on natural turbulent jets, i.e. turbulent jets without any artificial forcing. Attenuation of about 60% in fluctuation energy was obtained in the unforced jet case. It was also observed that the reduction of the wavepackets persisted further downstream of the control target location, for both the forced and unforced cases.

This study was motivated by positive results obtained from other previous works, such as the use of the Wiener-Hopf technique for the application in flow control, both numerically (Martini *et al.* 2022) and experimentally (Audiffred *et al.* 2023b), and the experimental control of forced jets using the IFFC method (Maia *et al.* 2021). Although the power spectra and phase differences of forced wavepackets are similar to what is found in unforced turbulent jets, the control of a natural jet becomes more challenging due to lower coherence levels, and they are a better representation of real applications. Furthermore, despite difficulties with feedback contamination of sensor readings and poor actuator performance at large bandwidths, control was found to be successful in generating substantial energy attenuation.

The placement of sensors had an important influence in the control of the natural jet. Once sensors were moved from  $x/D = 0.3$  to  $x/D = 0.58$ , better coherence levels with the downstream target sensor could be obtained, and with this, the far-field noise attenuation improved accordingly. Within this context, the Wiener-Hopf technique played a major role in order to deal with the non-causality observed in the IFFC kernels, leading to optimal control laws that were able to further reduce velocity fluctuations. Where we were able to reach a reduction of 28% of the velocity fluctuations in terms of RMS values, and a target frequency range-integrated energy reduction of 50%.

Although this control experiment was performed for a low Mach number, the control of a natural turbulent jet presented here is an important step towards the control of turbulent jets under

real flight conditions. Furthermore, the same sound radiation mechanisms are observed for higher Reynolds and subsonic Mach numbers, with sound radiation for low polar angles dominated by the axisymmetric mode (Cavaliere *et al.* 2012). Therefore, the control strategy adopted here, with an improvement of the experimental setup, could be extended to higher Mach numbers with further technological applications.

## 6. Acknowledgements

This work has received funding from the European Union's Horizon 2020 research and innovation programme under grant agreement No861438. We also wish to acknowledge the financial support from the Coordination for the Improvement of Higher Education Personnel (CAPES) and from the São Paulo Research Foundation (FAPESP), grants 2022/03279-5 and 2019/26546-6. We also acknowledge the technical support provided by Anton Lebedev, who greatly assisted the experiments conducted for this work.

## REFERENCES

- ALKISLAR, MEHMET B., KROTHAPALLI, A. & BUTLER, G. W. 2007 The effect of streamwise vortices on the aeroacoustics of a mach 0.9 jet. *Journal of Fluid Mechanics* **578**, 139–169.
- AUDIIFRED, DIEGO BONKOWSKI SIERRA, CAVALIERI, ANDRÉ V., JORDAN, PETER, MARTINI, EDUARDO & MAIA, IGOR 2023a *Wiener-Hopf approach applied for the control of forced turbulent jets*. American Institute of Aeronautics and Astronautics, arXiv: <https://arc.aiaa.org/doi/pdf/10.2514/6.2023-3880>.
- AUDIIFRED, DIEGO B. S., CAVALIERI, ANDRÉ V. G., BRITO, PEDRO P. C. & MARTINI, EDUARDO 2023b Experimental control of tollmien-schlichting waves using the wiener-hopf formalism. *Phys. Rev. Fluids* **8**, 073902.
- BELYAEV, I. V., BYCHKOV, O. P., ZAITSEV, M. YU., KOPIEV, V. A., KOPIEV, V. F., OSTRIKOV, N. N., FARANOSOV, G. A. & CHERNYSHEV, S. A. 2018 Development of the strategy of active control of instability waves in unexcited turbulent jets. *Fluid Dynamics* **53** (3), 347–360.
- BORGGAARD, JEFF, GUGERCIN, SERKAN & ZIETSMAN, LIZETTE 2016 Feedback stabilization of fluids using reduced-order models for control and compensator design. In *2016 IEEE 55th Conference on Decision and Control (CDC)*, pp. 7579–7585.
- BRITO, PEDRO P. C., MORRA, PIERLUIGI, CAVALIERI, ANDRÉ V. G., ARAÚJO, TIAGO B., HENNINGSON, DAN S. & HANIFI, ARDESHIR 2021 Experimental control of tollmien–schlichting waves using pressure sensors and plasma actuators. *Experiments in Fluids* **62** (2).
- CAVALIERI, ANDRÉ V. G., JORDAN, PETER, COLONIUS, TIM & GERVAIS, YVES 2012 Axisymmetric superdirectivity in subsonic jets. *Journal of Fluid Mechanics* **704**, 388–420.
- CAVALIERI, ANDRÉ V. G., JORDAN, PETER & LESSHAFFT, LUTZ 2019 Wave-packet models for jet dynamics and sound radiation. *Applied Mechanics Reviews* **71** (2), 020802–020802–27.
- CAVALIERI, ANDRÉ V. G., RODRÍGUEZ, DANIEL, JORDAN, PETER, COLONIUS, TIM & GERVAIS, YVES 2013 Wavepackets in the velocity field of turbulent jets. *Journal of Fluid Mechanics* **730**, 559–592.
- CROW, S. C. & CHAMPAGNE, F. H. 1971 Orderly structure in jet turbulence. *Journal of Fluid Mechanics* **48** (3), 547–591.
- DANIELE, V. & LOMBARDI, G. 2007 Fredholm factorization of wiener-hopf scalar and matrix kernels. *Radio Science* **42** (6), RS6S01.
- EUROPEAN COMMISSION 2011 *Flightpath 2050: Europe's vision for aviation: maintaining global leadership and serving society's needs*. Publications Office.
- FABBIANE, NICOLÒ, SIMON, BERNHARD, FISCHER, FELIX, GRUNDMANN, SVEN, BAGHERI, SHERVIN & HENNINGSON, DAN S. 2015 On the role of adaptivity for robust laminar flow control. *Journal of Fluid Mechanics* **767**, R1.
- FARANOSOV, GEORGY, BYCHKOV, OLEG P., KOPIEV, VICTOR, KOPIEV, VLADIMIR A., MORALEV, IVAN & KAZANSKY, PAVEL 2019 *Plasma-based active closed-loop control of instability waves in unexcited turbulent jet. Part 1. Free jet.*, arXiv: <https://arc.aiaa.org/doi/pdf/10.2514/6.2019-2557>.
- GINEVSKY, A. S., VLASOV, YE. V. & KARAVOSOV, R. K. 2004 *Reduction of Turbojet Engine Noise*, pp. 189–208. Berlin, Heidelberg: Springer Berlin Heidelberg.

- GUDMUNDSSON, K. & COLONIUS, TIM 2011 Instability wave models for the near-field fluctuations of turbulent jets. *Journal of Fluid Mechanics* **689**, 97–128.
- HERVÉ, AURELIEN, SIPP, DENIS, SCHMID, PETER J. & SAMUELIDES, MANUEL 2012 A physics-based approach to flow control using system identification. *Journal of Fluid Mechanics* **702**, 26–58.
- HUFF, DENNIS, HENDERSON, BRENDA, BERTON, JEFF & SEIDEL, JONATHAN 2016 Perceived noise analysis for offset jets applied to commercial supersonic aircraft. In *54th AIAA Aerospace Sciences Meeting*.
- HUFF, DENNIS L. 2007 Noise reduction technologies for turbofan engines. *Tech. Rep.*. National Aeronautics and Space Administration, Cleveland, Ohio 44135.
- JORDAN, PETER & COLONIUS, TIM 2013 Wave packets and turbulent jet noise. *Annual Review of Fluid Mechanics* **45** (1), 173–195, arXiv: <https://doi.org/10.1146/annurev-fluid-011212-140756>.
- JUVE, DANIEL, SUNYACH, MICHEL & COMTE-BELLOT, GENEVIEVE 1979 Filtered azimuthal correlations in the acoustic far field of a subsonic jet. *AIAA Journal* **17** (1), 112–113, arXiv: <https://doi.org/10.2514/3.61076>.
- KARBAN, UGUR, MARTINI, EDUARDO & JORDAN, PETER 2023 Modeling closed-loop control of installed jet noise using ginzburg-landau equation. *Flow, Turbulence and Combustion*.
- KOPIEV, V F, AKISHEV, Y S, BELYAEV, I V, BEREZHETSKAYA, N K, BITYURIN, V A, FARANOSOV, G A, GRUSHIN, M E, KLIMOV, A I, KOPIEV, V A, KOSSYI, I A, MORALEV, I A, OSTRIKOV, N N, TAKTAKISHVILI, M I, TRUSHKIN, N I & ZAYTSEV, M YU 2014 Instability wave control in turbulent jet by plasma actuators. *Journal of Physics D: Applied Physics* **47** (50), 505201.
- KOPIEV, V. F., BELYAEV, I. V., ZAYTSEV, M. YU., KOPIEV, V. A. & FARANOSOV, G. A. 2013 Acoustic control of instability waves in a turbulent jet. *Acoustical Physics* **59** (1), 16–26.
- KOPIEV, V. F. & FARANOSOV, G. A. 2008 Control over the instability wave in terms of the two-dimensional model of a nozzle edge. *Acoustical Physics* **54** (3), 319–326.
- LAJÚS, F. C., SINHA, A., CAVALIERI, A. V. G., DESCHAMPS, C. J. & COLONIUS, T. 2019 Spatial stability analysis of subsonic corrugated jets. *Journal of Fluid Mechanics* **876**, 766–791.
- LAU, J.C., FISHER, M.J. & FUCHS, H.V. 1972 The intrinsic structure of turbulent jets. *Journal of Sound and Vibration* **22** (4), 379–406.
- LEYLEKIAN, LAURENT, LEBRUN, MAXIME & LEMPEREUR, PIERRE 2014 An overview of aircraft noise reduction technologies. *AerospaceLab Journal* **Issue 7**, June 2014; ISSN: 2107–6596.
- LIGHTHILL, MICHAEL JAMES 1952 On sound generated aerodynamically i. general theory. *Proceedings of the Royal Society of London. Series A. Mathematical and Physical Sciences* **211** (1107), 564–587, arXiv: <https://royalsocietypublishing.org/doi/pdf/10.1098/rspa.1952.0060>.
- MAIA, IGOR A., JORDAN, PETER & CAVALIERI, ANDRÉ V. G. 2022 Wave cancellation in jets with laminar and turbulent boundary layers: The effect of nonlinearity. *Phys. Rev. Fluids* **7**, 033903.
- MAIA, IGOR A., JORDAN, PETER, CAVALIERI, ANDRÉ V. G., MARTINI, EDUARDO, SASAKI, KENZO & SILVESTRE, FLÁVIO J. 2021 Real-time reactive control of stochastic disturbances in forced turbulent jets. *Phys. Rev. Fluids* **6**, 123901.
- MARTINELLI, FULVIO 2009 Feedback control of turbulent wall flows. PhD thesis, Politecnico di Milano, Milão.
- MARTINI, EDUARDO, JUNG, JUNOH, CAVALIERI, ANDRÉ V.G., JORDAN, PETER & TOWNE, AARON 2022 Resolvent-based tools for optimal estimation and control via the wiener–hopf formalism. *Journal of Fluid Mechanics* **937**, A19.
- MICHALKE, A. 1983 Some remarks on source coherence affecting jet noise. *Journal of Sound and Vibration* **87** (1), 1–17.
- MOLLO-CHRISTENSEN, ERIK 1967 Jet Noise and Shear Flow Instability Seen From an Experimenter’s Viewpoint. *Journal of Applied Mechanics* **34** (1), 1–7, arXiv: <https://asmedigitalcollection.asme.org/appliedmechanics/article-pdf/34/1/1/5448018/1-1.pdf>.
- MOORE, C. J. 1977 The role of shear-layer instability waves in jet exhaust noise. *Journal of Fluid Mechanics* **80** (2), 321–367.
- MORRIS, PHILIP J. & McLAUGHLIN, DENNIS K. 2019 Noise and noise reduction in supersonic jets. In *Flinovia—Flow Induced Noise and Vibration Issues and Aspects-II* (ed. Elena Ciappi, Sergio De Rosa, Francesco Franco, Jean-Louis Guyader, Stephen A. Hambric, Randolph Chi Kin Leung & Amanda D. Hanford), pp. 85–96. Cham: Springer International Publishing.
- NOBLE, B 1958 Method based on the wiener-hopf technique for the solution of partial differential equations.
- PAEZANOVIĆ, VLADIMIR, LAURENTIE, JEAN-CHARLES, FOURMENT, CARINE, DELVILLE, JOËL, BONNET, JEAN-PAUL, SPOHN, ANDREAS, DURIEZ, THOMAS, CORDIER, LAURENT, NOACK, BERND R., ABEL, MARKUS, SEGOND, MARC, SHAQARIN, TAMIR & BRUNTON, STEVEN L. 2014 Mixing layer manipulation

- experiment: From open-loop forcing to closed-loop machine learning control. *Flow, Turbulence and Combustion* **94** (1), 155–173.
- SAIYED, NASEEM, BRIDGES, JAMES & MIKKELSEN, KEVIN 2000 *Acoustics and thrust of separate-flow exhaust nozzles with mixing devices for high-bypass-ratio engines*, arXiv: <https://arc.aiaa.org/doi/pdf/10.2514/6.2000-1961>.
- SANFILIPPO, DARIO & VALLE, ANDREA 2013 Feedback systems: An analytical framework. *Computer Music Journal* **37** (2), 12–27.
- SASAKI, KENZO, MORRA, PIERLUIGI, FABBIANE, NICOLO, CAVALIERI, ANDRÉ V.G., HANIFI, ARDESHIR & HENNINGSON, DAN S. 2018 On the wave-cancelling nature of boundary layer flow control. *Theoretical and Computational Fluid Dynamics* **32** (5), 593–616.
- SEINER, JOHN & KREJSA, EUGENE 1989 Supersonic jet noise and the high speed civil transport. In *AIAA, ASME, SAE, and ASEE, 25th Joint Propulsion Conference*.
- SHAQARIN, T, NOACK, B R & MORZYŃSKI, M 2018 The need for prediction in feedback control of a mixing layer. *Fluid Dynamics Research* **50** (6), 065514.
- SINHA, ANIRUDDHA, GUDMUNDSSON, KRISTJÁN, XIA, HAO & COLONIUS, TIM 2016 Parabolized stability analysis of jets from serrated nozzles. *Journal of Fluid Mechanics* **789**, 36–63.
- SUZUKI, TAKAO & COLONIUS, TIM 2006 Instability waves in a subsonic round jet detected using a near-field phased microphone array. *Journal of Fluid Mechanics* **565**, 197–226.
- TAM, CHRISTOPHER, GOLEBIEWSKI, MICHEL & SEINER, J. 1996 On the two components of turbulent mixing noise from supersonic jets. In *Aeroacoustics Conference*. American Institute of Aeronautics and Astronautics.
- TAM, CHRISTOPHER K. W., VISWANATHAN, K., AHUJA, K. K. & PANDA, J. 2008 The sources of jet noise: experimental evidence. *Journal of Fluid Mechanics* **615**, 253–292.
- TIDE, P S & SRINIVASAN, K 2009 Novel chevron nozzle concepts for jet noise reduction. *Proceedings of the Institution of Mechanical Engineers, Part G: Journal of Aerospace Engineering* **223** (1), 51–67, arXiv: <https://doi.org/10.1243/09544100JAERO347>.
- WANG, JINJUN & FENG, LIHAO 2018 *Synthetic Jet*, pp. 168–305. *Cambridge Aerospace Series*. Cambridge University Press.
- WEI, MINGJUN & FREUND, JONATHAN B. 2005 A noise-controlled free shear flow. *Journal of Fluid Mechanics* **546** (1), 123.
- WIRT, L. S. 1966 Gas turbine exhaust noise and its attenuation. *SAE Transactions* **74**, 762–784.
- ZIGUNOV, FERNANDO, SELLAPPAN, PRABU & ALVI, FARRUKH. S. 2022 Reduction of noise in cold and hot supersonic jets using active flow control guided by a genetic algorithm. *Journal of Fluid Mechanics* **952**, A40.